Developmental thyroid disruption permanently affects the neuroglial output in the murine subventricular zone

Pieter Vancamp, Karine Le Blay, Lucile Butruille, Anthony Sébillot, Anita Boelen, Barbara Demeneix, Sylvie Remaud

Developmental thyroid disruption permanently affects the neuroglial output in the murine subventricular zone

Pieter Vancamp[1], Karine Le Blay[1], Lucile Butruille[1], Anthony Sébillot[1], Anita Boelen[2], Barbara A. Demeneix[1], Sylvie Remaud[1*]

[1] Laboratory Molecular Physiology and Adaptation, CNRS UMR 7221, Department Adaptations of Life, Muséum National d'Histoire Naturelle, F-75005 Paris, France. [2] Endocrine Laboratory, department of Clinical Chemistry, Amsterdam UMC, University of Amsterdam, 1105 AZ Amsterdam, Netherlands.

Correspondance: *Sylvie REMAUD, PhD
Assistant Professor / Maître de Conférences MNHN
UMR 7221, CNRS/MNHN
Laboratory molecular physiology and adaptation
7 rue Cuvier, 75231 PARIS Cedex 5, France
+33 1 40 79 35 58
sremaud@mnhn.fr

Summary

Neural stem cells (NSCs) in the adult brain are a source of neural cells for brain injury repair. We investigated whether their capacity to generate new neurons and glia is determined by thyroid hormone (TH) during development, as serum levels peak during postnatal reorganization of the main NSC niche, the subventricular zone (SVZ). Re-analysis of mouse transcriptome data revealed increased expression of TH transporters and deiodinases in postnatal SVZ-NSCs, promoting local TH action, concomitant with a burst in neurogenesis. Inducing developmental hypothyroidism reduced NSC proliferation, disrupted expression of genes implicated in NSC determination and TH signaling, and altered neuro/glia outputs in newborns. Three-month-old adult mice recovering from developmental hypothyroidism had fewer olfactory interneurons and underperformed on short-memory odor tests, dependent on SVZ-neurogenesis. Our data provide read-outs permitting comparison with adverse long-term events following thyroid disruptor exposure, and provide ideas on the etiology of prevalent neurodegenerative diseases in industrialized countries.

Key words: Neural stem cells, Subventricular zone, Thyroid hormones, Developmental hypothyroidism, Cell fate, Olfaction, Single-cell RNA-Seq.

Introduction

Distinct regions in the adult mammalian brain harbor neural stem cells (NSCs) that proliferate well beyond development and sustain life-long generation of new neural cells. The largest area is the subventricular zone (SVZ) lining the lateral forebrain ventricles. Under physiological conditions in mice, SVZ-NSCs are primarily a source of neuroblasts, and less commonly, oligodendrocytes precursor cells (OPCs) (Menn et al., 2006). Neuroblasts migrate along the rostral migratory stream to integrate olfactory bulb networks, ensuring olfactory function (Lim and Alvarez-Buylla, 2016). OPCs populate nearby tissues, notably the corpus callosum, and differentiate into myelinating oligodendrocytes (Menn et al., 2006).

SVZ-NSCs originate from radial glia of the embryonic VZ-SVZ (Fuentealba et al., 2015; Merkle et al., 2004). A single-cell RNA-Seq analysis on mouse SVZ cells isolated throughout development

revealed that embryonically produced NSCs reactivate and acquire their definitive neurogliogenic identity between postnatal day 7 (P7) and P20 (Borrett et al., 2020), establishing a stable neuro/glia output thereafter. However, the factors governing this transition remain elusive. We hypothesized thyroid hormone (TH) could fulfil this role, as this endocrine cue also coordinates development of other brain regions (Williams, 2008). A postnatal TH peak conserved across the vertebrate lineage thereby coincides with the transition from a plastic, developmental state to a mature brain, both in terms of cyto-architecture and function (Gothié et al., 2020; Hadj-Sahraoui et al., 2000). Exposing rodents to hypothyroidism-inducing goitrogens dysregulated processes underlying corticogenesis, which, depending on the timing of exposure, include NSC proliferation, fate choice, migration and differentiation (Moog et al., 2017). In the subgranular zone of the hippocampal dentate gyrus, another important NSC zone where life-long neurogenesis modulates learning- and memory-dependent plasticity, hypothyroidism in rats from P10-P21 reduced cell proliferation and stalled neurogenesis up until P90, the latest investigated time point (Zhang et al., 2009). Structural alterations can be irreversible depending on the duration and the intensity of a hypothyroid insult, and negatively affect associated cognitive and motor skills in adult animals (Amano et al., 2018; Gilbert et al., 2017).

The biologically most active TH, 3,5,3'-triiodothyronine (T_3), modulates gene transcriptional activity through TH receptor α (TRα), to modulate NSC renewal and promote neuronal commitment in the adult mouse SVZ (Gothié et al., 2017; Lemkine et al., 2005; López-Juárez et al., 2012; Remaud et al., 2017). Increased intracellular T_3 in amplifying neuroprogenitors relieved arrested *Sox2* expression, favoring neuronal commitment (López-Juárez et al., 2012), while reduced T_3 action downregulated *Egfr*, favoring OPC fate (Remaud et al., 2017). Correspondingly, adult-onset hypothyroidism reduced the neuroblast output and increased OPC generation (Gothié et al., 2017). These observations in the adult mouse raised the question whether local TH signaling acts similarly to determine later-life NSC properties during postnatal SVZ development. Regulators of TH availability thereby confine T_3 action in a brain cell type-specific manner. These include the main TH transporters OATP1C1 taking up T_4, and MCT8 taking up both T_3 and T_4 (López-Espíndola et al., 2019; Roberts et al., 2008; Wilpert et al., 2020), deiodinase type 2 (DIO2) activating T_4 into T_3, and DIO3 inactivating T_3 and T_4 (Bárez-López

and Guadaño-Ferraz, 2017; Bianco et al., 2019). Discerning their expression patterns in the developing SVZ allows identifying TH-target cell populations and hence those potentially vulnerable to TH signaling disruption.

These questions are central in stem cell biology, as SVZ-NSCs are a potential source of new neurons and glia that could facilitate CNS injury repair (Vancamp et al., 2020a). Additionally, mounting evidence shows that developmental exposure to endocrine disrupting chemicals (EDCs) that alter TH homeostasis (Boas et al., 2012) evoke adverse, and sometimes irreversible effects on the fetal/postnatal brain (Mughal et al., 2018), but with a so far unknown impact on (SVZ-)NSCs. Epidemiological data already showed that slight variations in TH levels during fetal development not only reduce human offspring IQ, but also impair lineage decisions as reflected in altered grey/white matter ratios (Korevaar et al., 2016).

Here, we investigated TH regulator expression during postnatal SVZ remodeling by re-analyzing publicly available single-cell RNA-Seq data and using RNAscope. Then, we sought out how ablating the postnatal TH peak by 6-n-propyl-2-thiouracil (PTU)-induced hypothyroidism affects the murine SVZ in the short- and long-term, in particular neuro/glial output and olfactory behavior. We identified the developing SVZ as a tissue sensitive for aberrant TH signaling, pinpointing various processes of interest when studying the impact of EDCs.

Results

TH regulators are dynamically expressed in the postnatal SVZ.

To grasp how TH availability is regulated in different SVZ cell types before and after the TH peak, we re-analyzed single-cell RNA-Seq data obtained from P2- and P20-SVZ cells of *Emx1-Cre;R26-LSL-EYFP* mice (Borrett et al., 2020) using the Seurat v3.0 toolkit (Stuart et al., 2019). Following integration and two-dimensional reduction, we plotted SVZ cell type-specific markers (Zywitza et al., 2018) and isolated 12 cell clusters (**Fig. S1**). Five were of interest for our study, recapitulating neuronal *vs.* glial lineages: NSCs, transient amplifying progenitors (TAPs), glia (astrocytes, OPCs),

and neuroblasts (**Fig. 1A**). Astrocyte and NSC proportions at P20 were higher than at P2, at the expense of TAPs and neuroblasts. OPC numbers remained stable (**Fig. 1A**).

We then examined expression of TH regulators and neuroglial cell markers within these isolated cell populations. *Dio2* was mainly enriched in a subpopulation of astrocytes, and in some NSCs at P20. Some NSCs also expressed *Dio3* (**Fig. 1B**). *Thra*, encoding TRα1 and TRα2, was ubiquitously expressed in SVZ cells at P2 and P20, whereas *Thrb* was in only a few cells across the different categories (**Fig. 1B, Fig. S2**), as expected (Lemkine et al., 2005). Compared to P2, many NSCs increasingly expressed *Oatp1c1*, and to a minor extent, *Mct8* at P20. Astrocytes predominantly expressed *Oatp1c1* at P20 (**Fig. 1B**). Yellow colors on the cluster plots show *Mct8* and *Oatp1c1* overlapping in an important fraction of SVZ-NSCs and astrocytes at P20 (**Fig. 1C, Fig. S2**). Almost none of the *Dio3*+ cells co-expressed neither of the TH transporters (**Fig. S3**). Several neuroblasts also expressed *Mct8*, but only at P2 (**Fig. 1B, C**). At P20, both transporters were also enriched in epithelial and endothelial cells forming the blood-cerebrospinal fluid and blood-brain barrier (BBB), respectively (**Fig. S4**). Absence of endothelial cell expression at P2 suggests TH uptake in the SVZ occurs via BBB-independent routes before the TH peak.

Expression of the positively regulated T_3-target gene *Krüppel-like factor 9* (*Klf9*) (Dugas et al., 2012) was higher at P20, while the negatively regulated *Musashi-1* (*Msi1*) (López-Juárez et al., 2012) displayed an inverse pattern (**Fig. 1D, Fig. S2**). Among the neuroglia markers, *Olig2* was enriched in P2 astrocytes, and in OPCs in which a concomitant rise in *Ng2* corresponded to a postnatal wave of oligodendrogenesis (Vancamp et al., 2020b) (**Fig. 1D**). As expected, *Dlx2* and *Dcx* marked early committed neuroprogenitors and neuroblasts, respectively. Few *Dlx2*+ NSCs indicated neuronal lineage commitment while their transcriptional profile still assigned a stem cell identity.

To validate *in silico* data, we combined RNAscope, visualizing single mRNA transcripts, to SOX2 IHC at P4 and P21, a marker of progenitor pluripotency, on coronal SVZ sections (**Fig. 1E,F**). Average *Thra*, *Klf9* and *Mct8* mRNA transcript numbers increased in the majority of SOX2+ cells (**Fig. 1F**) as observed before (**Fig. 1B-D**), whereas cellular *Dio3* expression remained low from P4 to

P21. IHC showed this coincided with elevated TRα1 levels in SOX2+ SVZ-progenitors after the TH peak (**Fig. 1G**).

Overall, the dynamically increased TH regulator expression in SVZ-NSCs and astrocytes after the TH peak suggests they are primary TH targets and possess all molecular machinery to promote TH action during postnatal SVZ reorganization.

Developmental hypothyroidism alters TH regulator and neuroglia gene expression in the postnatal SVZ.

Then, to study how ablation of the TH peak affects cellular TH signaling and neuroglia commitment, we fed dams a 0.15% PTU-enriched diet that blocks TH synthesis, exposing the progeny from E15-P21. Newborn weighed less at P15-P21 (Šidák following two-way ANOVA, $F_{1,48}$=115.7, p<0.0001) (**Fig. 2A**). Serum T_4 and T_3 levels in PTU-treated P4 and P15 mice were lower than the mass-spectrometry detection threshold (<0.2 and <0.1 nmol/L, respectively), while concentrations peaked in P15 control animals (**Fig. 2B**).

We then examined expression of genes associated with TH signaling and neuroglia commitment in dissected SVZs from P4-P21. A heat-map depicts the relative change in gene expression compared to P4 controls for each gene (**Fig. 2C;** fold changes in **Table S1).** In normal conditions, rising *Dio2*, *Oatp1c1* and *Klf9* over the course of postnatal development indicated increased TH action.

When comparing numbers of the in total 13 tested genes between controls *vs.* PTU-treated SVZs, 2 were up- and 7 were downregulated at some point, with a maximum of 6 differentially expressed genes at P15. Only at P4, no genes were affected. Increased *Dio2* (Two-way ANOVA, $F_{1,30}$=19.32, p=0.0001) together with decreased *Dio3* expression ($F_{1,30}$=28.11, p<0.0001) are classic signs of hypothyroidism (Hernandez et al., 2012), and confirm low TH levels in SVZ tissues from P8 onwards (**Fig. 2C**).

At P15, 4 key neurogliogenic genes were downregulated: the multipotent NSC/progenitor marker *Sox2* (Šidák following two-way ANOVA, t_{30}=3.705, p=0.0034), *Dlx2* (t_{30}=3.464, p=0.0065), *Dcx* (t_{30}=2.977, p=0.0226), and the oligodendroglial cell marker *Olig2* (t_{30}=4.116, p=0.0011). The latter

was still downregulated at P21 (t_{30}=3.639, p=0.0041), whereas it gradually increased in control conditions (**Fig. 2C**). By combining RNAscope with IHC at P21 and counting single mRNA transcripts in randomly selected SOX2+ cells, we confirmed upregulated *Dio2* (t-test, t_5=4.377, p=0.0072), and downregulated *Dio3* (Mann-Whitney U test, p=0.029) and *Klf9* (t-test, t_6=3.427, p=0.014) in SVZ-progenitors of PTU-exposed mice (**Fig. 2D**).

These results indicate that developmental hypothyroidism alters transcription patterns of TH-responsive genes and those involved in NSC/TAP maintenance and commitment.

Developmental hypothyroidism alters neurogliogenesis in the postnatal SVZ.

We then studied SVZ-neuroblast and -OPC generation, before (P4) and after the TH peak (P21), using antibodies against DCX and OLIG2, respectively (**Fig. 3A**). We distinguished between the dorsal and lateroventral (LV) SVZ as recent data demonstrated these microdomains have different neuroglia outputs (e.g. (Mizrak et al., 2019)). In both conditions, almost exclusively OLIG2+ OPCs were generated at P4, while a burst in DCX+ neuroblasts was observed at P21 in both microdomains (**Fig. 3B**). The OPC density in the dorsal SVZ was similar as a function of age (Two-way ANOVA, $F_{1,21}$=1.678, p=0.21) and not affected by hypothyroidism ($F_{1,21}$=0.011, p=0,92). In contrast, the density of DCX+ neuroblasts was 40% lower in P21 PTU-treated animals (Tukey following two-way ANOVA, q_{21}=8.36, p<0.0001).

The LV-SVZ was thinner in hypothyroid conditions (Tukey following two-way ANOVA, P4: q_{17}=4.921, p=0.014; P21: q_{17}=4.154, p=0.041) (**Fig. 3C**). At P21, OLIG2+ cell numbers in PTU-treated animals were only one-tenth of controls (Tukey following two-way ANOVA, q_{21}=6.67, p=0.0006). DCX+ neuroblasts numbers increased from P4 to P21, and were reduced by PTU at P21 (q_{21}=4.05, p=0.043) (**Fig. 3D**). Hence, developmental hypothyroidism reduces postnatal neurogenesis in the P21 SVZ and oligodendrogenesis in the LV-SVZ.

Lastly, we calculated the proportion of DCX+/OLIG2+ cells reflecting the neuro/glia balance (**Fig. 3E**). As observed with IHC, the dorsal SVZ output was predominantly gliogenic at P4. At P21 however, more than 80% of committed cells was DCX+. The neuro/glia ratio in the dorsal SVZ did

not change in hypothyroid conditions (Two-way ANOVA, $F_{1,21}$=0.769, p=0.39). In the LV-SVZ, the neuro/glia ratio changed from 62/28% to 90/10% at P21, following PTU exposure (Tukey following two-way ANOVA, q_{21}=8.10, p<0.0001) (**Fig. 3E**).

Developmental hypothyroidism reduces postnatal SVZ-NSC proliferation and increases the progenitor pool.

Next, we assessed progenitor behavior using antibodies against SOX2 to label NSC/progenitors, and PH3 for mitotic cells (**Fig. 4A**). In the dorsal SVZ, SOX2+ cell densities were respectively more than 2- and 3-fold higher in PTU conditions at P4 (Tukey following two-way ANOVA, q_{19}=4.88, p=0.013) and P21 (q_{19}=9.08, p<0.0001), as compared to controls (**Fig. 4A,B**). Densities of PH3+ cells were reduced 2-fold in hypothyroid conditions at P21 (Tukey following two-way ANOVA, q_{19}=5.05, p=0.011), but not at P4 (q_{19}=1.86, p=0.57) (**Fig. 4B**).

In the LV-SVZ, SOX2+ cell numbers were 2-fold higher following PTU exposure, at P4 only (Tukey following two-way ANOVA, q_{19}=6.60, p=0.0009). PH3+ cell numbers were lower at P4 (Tukey following two-way ANOVA, q_{19}=6.10, p=0.0019) and P21 in PTU *vs.* controls (q_{19}=4.80, p=0.015) (**Fig. 4C,D**). These data show that postnatal SVZ-progenitors proliferate less in hypothyroid conditions, while a larger progenitor pool suggests a blocked cell cycle, as expected (Lemkine et al., 2005).

***In vitro* neurospheres prepared from PTU-treated P21 newborns are less responsive to T_3.**

Next, we prepared *in vitro* neurospheres from dissected SVZs of control and PTU-treated mice, allowed them proliferate for 7 days, and then differentiate for 7 days ± 1 or 50 nM exogenous T_3 (**Fig. 5A**).

At P4, around 5% of the SVZ-progenitors dissected from control or PTU-treated mice were OLIG2+ and 40% were DCX+, a ratio that did not change under added T_3 (**Fig. 5B,C**). However, at P21, T_3 treatment increased proportions of OLIG2+ OPCs in neurospheres derived from control animals (10 vs. 5%, Tukey following two-way ANOVA, q_{161}=6.159, p=0.0003), but not in those dissected from PTU-treated animals (q_{161}=3.255, p=0.199) (**Fig. 5D,E**). Similarly, the proportion of DCX+ cells

decreased after T_3 treatment, but only in neurospheres prepared from control animals (18 vs. 33%, q_{161}=6.887, p<0.0001). Consequently, DCX+ proportions were lower under 50 nM T_3 treatment in neurospheres prepared from PTU-treated animals as compared to controls (q_{161}=4.366, p=0.0282).

As a result, in neurospheres prepared from control P21 mice, the neuro/glia balance decreased by 22% following addition of 50 nM T_3 (Tukey following two-way ANOVA, q_{161}=8.752, p<0.0001), but did not change in cells cultured from PTU-treated mice (q_{161}=3.571, p=0.123) (**Fig. 5F**). In other words, the neuro/glia ratio in 50 nM T_3-treated cell cultures derived from control P21 mice changed from 83%/17% to 61%/39%, while remaining at ±80%/20% in cultures of PTU-treated P21 mice. These results suggest that SVZ-NSC/progenitors are particularly sensitive to T_3 after the TH peak, echoing our *in vivo* data. They lose their responsiveness to T_3 following developmental hypothyroidism.

A transient developmental hypothyroidism persistently impairs SVZ neurogliogenesis and behavior in adult mice.

Lastly, we examined P100 mice that were fed a normal diet after PTU exposure from E15-P21. Adult mice developmentally treated with PTU did not reach a normal weight (t-test, t_8=3.158, p=0.0134) (**Fig. 6A**). Mass-spectrometry analysis revealed normalization of serum T_4 levels (t-test, t_8=0.330, p=0.75), but borderline-significantly lower T_3 (t_8=2.141, p=0.0647), and increased reverse T_3 (rT_3) levels (Mann-Whitney U test, p=0.0159) (**Fig. 6A**), suggesting persistent thyroid axis alterations.

A last set of experiments analyzed long-lasting consequences on NSC fate and associated behavior. Olfactory memory in mice relies on a supply of SVZ-derived neuroblasts (Lim and Alvarez-Buylla, 2016). Adult mice underwent an olfactory habituation-dishabituation test with five odors (**Fig. 6B**). The investigation time of an odor indicated their ability to habituate, and dishabituate each time a new odor was presented. Developmentally PTU-treated mice lost their preference for female urine as to when male urine was presented (Bonferroni following two-way ANOVA, t_{60}=8.328, p<0.001). Apart from that, all mice successfully discriminated other odors.

Then, we measured the investigation time 2, 30 and 60 min after presenting an odor to assess short-term olfactory memory. In control mice, investigation time dropped with each presentation (i.e.

habituation). In developmentally PTU-treated mice, investigation time increased again 30 min after the second, and 60 min after the third presentation, differing significantly from control animals (Bonferroni following two-way ANOVA, 30 min: t_{16}=4.321, p=0.0021; 60 min: t_{16}=9.056, p<0.001) (**Fig. 6C**). This indicates that the ability to remember an odor over a short period is impaired in adult mice that were developmentally exposed to PTU.

To identify the cellular effects underlying this phenotype, we performed IHC for three key interneurons in the olfactory bulbs of the same mice: calretinin, calbindin and tyrosine hydroxylase (**Fig. 6D**). The density of tyrosine hydroxylase+ neurons in the glomerular layer was significantly decreased (Mann-Whitney U test, p=0.0317), as was that of calretinin+ neurons (t-test, t_8=3.434, p=0.0089), and borderline-significantly for calbindin+ neurons (t-test, t_8=2.098, p=0.069) (**Fig. 6E**). Cell type proportions were unaltered.

We also assessed the cellular processes we previously examined (**Fig. 7A**). The SVZ area was 20% smaller at P100 in mice developmentally exposed to PTU (graph not shown, t_8=2.463, p=0.039). DCX+ cell densities in the dorsal (t-test, t_8=0.4327, p=0.68) and LV-SVZ (t-test, t_8=1.297, p=0.23) were similar in both groups. However, as the SVZ was smaller, absolute neuroblast numbers were lower in developmentally PTU-exposed mice. OLIG2+ cell densities were almost 2-fold lower in the dorsal (t-test, t_8=2.926, p=0.019) and LV-SVZ of adult mice developmentally exposed to PTU (t-test, t_8=3.112, p=0.014) (**Fig. 7B**). This drop increased the neuro/glia balance in the dorsal SVZ from 86%/14% to 93%/7% (t-test, t_8=3.247, p=0.012) whereas it did not change in the LV-SVZ (**Fig. 7C**). These data indicate that SVZ-neurogenesis in adult mice developmentally exposed to PTU recovers, but SVZ-oligodendrogenesis remained impaired.

We also stained for SOX2 and PH3, as well as Ki67 to detect cycling cells (as in (Vancamp et al., 2019)) (**Fig. 7D**). SOX2+ cell numbers were 30% lower in the LV-SVZ of developmentally PTU-exposed mice (t-test, t_8=2.901, p=0.020). Ki67+ and PH3+ cell numbers did not differ between conditions or SVZ microdomains (**Fig. 7E**). The proliferation index, the proportion of PH3+ cells in the Ki67+ population, did not change, suggesting that the cell cycle was unaffected by developmental PTU exposure (**Fig. 7F**).

Discussion

The adult SVZ harbors the largest NSC population that generates new neuroblasts and OPCs throughout life. A single-cell RNA-Seq analysis on mouse SVZ cells isolated throughout development estimated that NSCs, produced during embryonic development (Fuentealba et al., 2015), reactivate postnatally and acquire their future neurogliogenic identity between P7-P20 (Borrett et al., 2020), establishing a stable neuro/glia output thereafter. Which factors govern this transition remains elusive. We hypothesized TH could be one of them, given that serum TH levels rise postnatally and peak at P15 (Hadj-Sahraoui et al., 2000), TH orchestrates NSC processes underlying brain development (Moog et al., 2017), and TH controls NSC proliferation and fate choice in the adult mouse SVZ (Lemkine et al., 2005; López-Juárez et al., 2012).

First, we re-explored the single-cell RNA-Seq data generated from *Emx1-Cre;R26-LSL-EYFP* mice (Borrett et al., 2020). Compared to P2, SVZ-NSC and astrocyte population sizes were ten times larger at P20, while TAP numbers had decreased, reflecting the characteristic adult SVZ composition with few cycling progenitors. High *Dio2* levels in P20 astrocytes suggested increased conversion of T_4 into T_3, facilitating T_3 supply to NSCs enriched with *Mct8* and *Oatp1c1*. At P20, brain-barriers cells were detectable too, and expressed *Mct8* and *Oatp1c1* as shown before (Roberts et al., 2008; Wilpert et al., 2020), indicating TH uptake from the blood and cerebrospinal fluid to SVZ cells is put in place during the first postnatal weeks.

Our IHC data showed that this postnatal transition occurs simultaneously with a burst in neuroblasts, generating a stable neuro/glia output of 80%/20%, characteristic of adult mice (Remaud et al., 2017; Zhang et al., 2009). The discrepancy between decreasing *Dcx* transcripts and more DCX+ neuroblasts from P4-P21 (**Fig. 2C** *vs.* **3A**), might reflect post-transcriptional mRNA repression in perinatal NSCs until molecular cues trigger translation into proteins. Similarly, some adult mouse SVZ cells expressed *Ttr*, while the encoding protein was undetectable (Vancamp et al., 2019). Sequencing individual mRNAs showed that NSC differentiation into neurons coincides with a dynamically changed translation of specific mRNAs and repression of *Sox2* (Baser et al., 2019), a key TH-responsive gate-keeper of NSC identity (López-Juárez et al., 2012). Such mechanisms bolster the hypothesis that the

embryonically generated NSC pool (Fuentealba et al., 2015) reactivates postnatally to establish neuroglial identities (Rushing and Ihrie, 2016), with TH potentially exerting a key role through pathways such as Wnt/β-catenin (Skah et al., 2017) and Notch (Aguirre et al., 2010).

We subsequently investigated whether postnatal TH deficiency disrupts SVZ organization, and thereby neuroglial processes. We focused on the neuro/glia balance, as T_3-TRα1 represses *Sox2* to favor neuronal commitment in adult NSCs (López-Juárez et al., 2012), and because this read-out is a relevant indicator for how well NSC/progenitors might respond to brain injury (Vancamp et al., 2020a). qPCR and RNAscope data showed downregulated expression of markers associated with neuroglial commitment, as well as TH-target genes *Klf9* and *Dio3* as a response to low intracellular T_3. This was most profound at P15-P21, during and after the TH peak, again suggesting that SVZ-NSCs respond to TH from then on. Correspondingly, before the peak at P4, we found no *in vivo* effects of PTU on neuroblast nor OPC generation. Absence of TH regulators at P2 as shown by single-cell RNA-Seq, suggested a lack of cellular machinery to respond to T_3. At P21 however, neuroblast densities in the dorsal SVZ alongside with *Dlx2* and *Dcx* expression decreased in PTU conditions, although OPC generation remained stable. SVZ-neurogenesis was also decreased in adult mice null for *Ttr* or exposed to methimazole, but they displayed increased OPC numbers (Gothié et al., 2017; Remaud et al., 2017; Vancamp et al., 2019). Similarly, hippocampal neurogenesis was reduced in mice developmentally exposed to PTU (E6-P21) or methimazole (P10-P21) (Gilbert et al., 2017; Zhang et al., 2009), or null for *Mct8* (Mayerl et al., 2020). Decreased *Olig2* expression was probably linked to reduced OPC generation in the LV-SVZ at P21. Hence, TH determines neurogliogenesis in stem cell zones of the murine brain from early stages onwards.

Remarkably, we found that 3-month-old mice, developmentally exposed to PTU but fed a normal diet from P21, had reduced OPC numbers and an altered neuro/glia ratio in the dorsal SVZ. Similarly, adult *Ttr* knockout mice that recovered from a delayed brain development (Monk et al., 2013), still had decreased SVZ neuro/glia ratios (Vancamp et al., 2019). Adult rats gestationally and perinatally treated with PTU also presented with heterotopia and aberrant cortical layering (Ausó et al., 2004; O'Shaughnessy et al., 2018). These anomalies relate to our *in vitro* results showing that NSCs cultured

306 from P21 PTU-treated mice responded less to exogenous T_3 in contrast to those from control mice,
307 indicating persistent alterations. Surprisingly, the T_3-dependent reduction in neuronal differentiation in
308 cultured control SVZ-NSCs did not corroborate with our findings that blocked T_3 action decreased
309 neuroblast generation *in vivo* (**Fig. 3A** *vs.* **5B**). In the hypothyroid adult murine SVZ, DCX+
310 neuroblast generation was also reduced, but a T_3-regimen enhanced neuronal differentiation in
311 cultured SVZ-NSCs from control animals (Gothié et al., 2017). This suggests that SVZ-NSCs behave
312 differently *in vitro* when cultured during development as opposed to adult stages, or due to missing
313 factors otherwise present *in vivo*. Additionally, TH regulator expression might respond different to
314 treatments *in vitro*. Nevertheless, the results indicate developmental endocrine perturbation disrupts
315 pathways underlying postnatal SVZ reorganization, misprogram NSCs permanently, and result in
316 abnormal neuro/glia outputs later in life. In addition, while adult mice were normothyroxinemic, lower
317 serum T_3 and higher rT_3 indicated repercussions on the thyroid axis and deiodinase activity as well,
318 and might aggravate inadequate TH availability control and signaling in tissues.

319 We also found more SOX2+ and less proliferating cells at P4-P21. Although TH negatively regulates
320 *Sox2* (López-Juárez et al., 2012), decreased expression of the gene in PTU-treated newborns could be
321 explained by cellular hypoplasia, as observed at P21 and later too, a consequence of reduced
322 proliferation, and maybe increased apoptosis. In developmentally PTU-exposed adult mice, the
323 progenitor pool in the LV-SVZ was still smaller, mimicking reduced SVZ- (Lemkine et al., 2005) and
324 SGZ-progenitor self-renewal following adult-onset hypothyroidism (Montero-Pedrazuela et al., 2006),
325 in both cases rescued by TH treatment. As SOX2 normally precedes oligodendroglial commitment
326 (Zhang et al., 2018), it may explain lower oligodendroglia numbers in the LV-SVZ. Another study
327 found no effect on the SVZ-NSC pool size in P90 mice exposed to PTU from P10-P21 (Zhang et al.,
328 2009). Either the treatment period was too short to produce visible effects, or TH affects NSC pool
329 expansion primarily between E15-P10. Previous rodent studies have already shown how the timing of
330 goitrogen exposure determines whether a specific developmental brain malformation is detectable or
331 not (O'Shaughnessy et al., 2018).

SVZ-NSCs are susceptible to endocrine perturbation during crucial developmental windows jeopardizing their future neurogliogenic properties. In the olfactory bulbs, the intertwined network of neuronal subtypes in the glomerular layer regulating olfaction was less densely populated, while relative proportions remained stable. As a result, adult mice failed to remember pure and distinct odors, a function dependent on adequate adult SVZ-neurogenesis (Breton-Provencher et al., 2009). *Mct8/Oatp1c1* double knockout mice displayed a similar behavioral phenotype, underlining the crucial role of TH transporters therein (Luongo et al., 2021). Similar impaired processes can explain why adult hypothyroid Kunming mice (Tong et al., 2007) also underperformed on short-term odor memory tests, although we cannot exclude side-effects of the PTU treatment on brain development as a whole.

Reduced OPC generation could adversely modify the generation of mature oligodendrocytes that promote myelin turnover (McKenzie et al., 2014) or might undermine remyelinating capacities in myelin-destructive diseases such as multiple sclerosis. Misprogrammed SVZ-NSCs could respond inadequately to brain injury, preventing repair through insufficiently replacing lost cells (Jacobs et al., 2017). Furthermore, different phenotypes between the dorsal and LV-SVZ suggest that factors encoded by TH-responsive genes fine-tune neuro/glia outputs differently across the microdomains (Mizrak et al., 2019), some of which might be linked to gradient expression of extracellular components such as *Wnt* (Azim et al., 2014) and *Shh* (Ihrie et al., 2011).

In conclusion, TH is a key factor determining early NSC identity and later-life SVZ-neuro/glia output in mice. Consequently, thyroid perturbation during critical windows of SVZ remodeling can reverberate long thereafter. The affected processes represent new read-outs that could be used to evaluate the long-term impact of developmental EDC exposure on the brain, as clear-cut indicators are currently lacking (Ramhøj et al., 2020). Exposing mice to 100 mg/kg of the TH-disruptor decabromodiphenyl ether from E6-P16, impaired NSC proliferation, SVZ-neurogenesis and reduced calretinin interneurons in the olfactory bulbs at P16 (Xu et al., 2018). Decreased grey/white matter in human offspring reflecting altered lineage decisions in the cortex, have also been linked to altered circulating maternal TH levels (Korevaar et al., 2016). Furthermore, our data bring new insights to understand how early-life thyroid disruption can compromise later-life intellectual capacity, linking

this with the alarming rise in several childhood (Gyllenberg et al., 2016) and maybe adult neurological disorders as well.

Experimental procedures

Single-cell RNA-Seq

Single-cell RNA-Seq analysis was performed on publicly available datasets of *Emx1-Cre;R26-LSL-EYFP* C57BL/6J mice ((Borrett et al., 2020), GEO accession number: GSE152281). High-throughput transcriptomic profiles were obtained using Illumina HiSeq 2500 on a 10X genomic platform. Two objects "P2-SVZ" (GSM4610595) and "P20-SVZ" (GSM4610600) were created using the Seurat v3.0 package in R-Studio 4.1.6 (Stuart et al., 2019). Data were log-normalized and variable features selected with FindVariableFeatures() (including variance stabilizing transformation, nfeatures=2000). Anchors were identified with FindIntegrationAnchors() prior to integrating datasets with IntegrateData(). Principal component analysis scaled and reduced data. A non-linear Uniform Manifold Approximation and Projection (UMAP) dimensional reduction (dim=1,20) allowed to cluster cell populations with FindClusters() (resolution=0.5). FeaturePlot() visualized expression of validated markers for murine SVZ-cell types (Zywitza et al., 2018) allowing to identify and annotate cell clusters (**Fig. S1**). The Subset() function was used to select clusters. Downstream analyses included gene expression visualization with FeaturePlot() and VlnPlot() (split.by= P2 vs. P20). Co-expression plots were obtained with the Overlay()=TRUE function.

Animals

Pregnant C57Bl/6J mice (day E11, Janvier labs, France) were housed at 22 °C and free access to water and food. Newborns were weaned at P21. Hypothyroidism was induced by giving dams iodine-free pellets containing 0.15% PTU during a period corresponding to E15-P21 for the progeny. Mice were sacrificed via cervical dislocation. Trunk blood (N=3/pool) was spinned down (3000 rpm, 25 min) to collect and store plasma at -20 °C. For qPCR, the SVZ was dissected on ice, snap-frozen and stored at -80 °C. For IHC, brains were fixed in 4% paraformaldehyde (PFA) in PBS overnight (4 °C), then in PBS 30% sucrose overnight, and embedded in Tissue-Tek® O.C.T.™ (Sakura Finetek, The

Netherlands). Coronal sections (12 µm) were made on a cryostat. All experiments were approved by the CNRS ethical board and performed in strict accordance with the European Directive 2010/63/EU.

Serum thyroid hormone concentrations

Serum TH concentrations were measured by UPLC-MS/MS (Ackermans et al., 2012) with minor adaptations to the sample pretreatment (de Vries et al., 2019). Briefly, 10 µL of standards in a 6% BSA matrix, serum controls and samples were diluted with 300 µL PBS and used. Detection limits were 0.2 nmol/L for T_4 and rT_3, and 0.1 nmol/L for T_3.

Neurosphere cultures

The procedure is described in the Supplemental Information.

RNA extraction and qPCR

The procedure is described in the Supplemental Information.

RNAscope

mRNA transcripts were stained on cryosections using the RNAscope® Multiplex Fluorescent Reagent Kit v2 Assay (Nr° 323100-USM, Advanced Cell Diagnostics, Hayward, CA, USA). RNAscope was performed first, excluding post-fixing tissue and protease III treatment (as in (Baser et al., 2019)). Slides were baked 60 min at 60 °C, dehydrated (50→70→100% EtOH), treated 10 min with H_2O_2 and incubated in Target Retrieval Reagent for 15 min at 98 °C. The next steps were performed using the HybEZ™ II Oven at 40 °C (as in (Vancamp et al., 2019)). Probes (Probe-Mm-*Dio3*-O1 (Cat# 562871); Probe-Mm-*Slc16a2*-C3 (Cat# 545291-C3); Probe-Mm-*Thra*-C2 (Cat# 519421-C2); Probe-Mm-*Klf9*-C2 (Cat# 488371-C2), ACD technologies) were incubated for 2 h. Positive (Probe-Mm-*Ubc*) and negative (Probe-Mm-*DapB*) controls were included. Sections were then incubated with Multiplex FL v2 Amp1 (30 min), Amp2 (30 min), and Amp3 (15 min). Fluorescent signal was developed by consecutive incubation with HRP-C1 (15 min) (ACD technologies), Opal™ 570 or 690 (1/750 in TSA-Amp diluent, Akoya Biosciences) (30 min), and HRP blocker (15 min) (ACD technologies). Slides were rinsed in 1X TBS + 0.2% Tween-20 prior to IHC.

410 **Immunohistochemistry**

411 The procedure is described in the Supplemental Information.

412 **Imaging and quantification**

413 Using a Leica TCS-SP5 confocal microscope (ImagoSeine, Université René Diderot), pictures were
414 taken of the olfactory bulbs, corpus callosum, the dorsal and LV-SVZ on 3-4 sections per mouse.
415 DAPI+ cells represented total cell numbers, allowing calculating proportions of marker-expressing
416 cells. For RNAscope, each dot represented a single mRNA transcript. On 4 pictures of the dorsal SVZ
417 per animal, transcript number/cell was counted in randomly selected 20 SOX2+ cells per picture. For
418 neurospheres, 10 pictures (370x370 µm²) of each replicate from each condition were taken. Counting
419 was done with the Cell Counter plugin in FIJI.

420 **Behavioral tests**

421 Mice first habituated to the cotton swab and a fresh cage for 15 min. The habituation-dishabituation
422 test comprised the presentation of 5 different odors (water, lemon, orange blossom, male & female
423 urine). Investigation time (the relative time mice spent in close proximity (±1 cm) of the cotton wool)
424 was measured following three consecutive presentations of 2 min with 1-minute intervals. A short-
425 term memory test measured the investigation time for 5 min after presenting mice with an odor after 0,
426 2, 30 and 60 min.

427 **Statistical analysis**

428 Data were analyzed with GraphPad Prism v9.00. Normality was tested using the Shapiro-Wilk
429 normality test and equality of variances was checked using the F test. Grubb's test detected possible
430 outliers. Whenever the criteria for parametric testing were unmet, non-parametric alternatives were
431 indicated. In case of normal distribution, an unpaired, two-tailed t-test compared means of two groups,
432 otherwise we used a Mann-Whitney U test. With two independent variables, a two-way ANOVA was
433 performed followed by a Tukey post-hoc tests when significant. Gene expression was evaluated with
434 two-way ANOVAs on Log-transformed data, followed by a Šidák post-hoc tests. Matched values of

behavioral tests were analyzed by two-way ANOVAs followed by Bonferroni post-hoc tests. "n" refers to the number of animals (i.e. biological replicates), N to the number of technical replicates. Culture experiments were conducted three times (n = 3), and 10 pictures were taken per well. P-values <0.05 were considered significant. Data are shown as scatter plots and bars depicting mean ± standard deviation, as a heat-map for qPCR, and violin or cluster plots for single-cell RNA-Seq data. Asterisks/letters indicate statistical significance.

Data and code availability

The GEO accession number for the single-cell RNA-seq data that were analyzed in this paper is: GSE152281.

Acknowledgements

We thank the ImagoSeine plateform of the Institut Jacques Monod (Université René Diderot). We also thank Fabien Uridat and Stéphane Sosinsky for excellent animal care. Pieter Vancamp was supported by the European Thyroid Association (basic science grant) and the Fondation pour la Recherche Médicale (Grant: SPF201909009111). This work was additionally supported by the Centre National de la Recherche Scientifique (CNRS) and the Muséum National d'Histoire Naturelle (MNHN), NeurATRIS (IONESCO grant), and the EU H2020 contract ATHENA (Grant n°666869).

Author contributions

S.R., B.D. and P.V. designed the study. P.V. performed the single-cell RNA-Seq re-analysis. A.B. performed the TH measurements. P.V. and K.L performed and analyzed qPCR and IHC experiments. P.V. performed RNAscope experiments. P.V., K.L. and A.S. did the *in vitro* experiments. L.B. did the behavioral studies. A.S. and S.R. assisted in dissections. P.V. collected, statistically analyzed and interpreted the final data. P.V. made the figures and wrote the manuscript together with S.R. and B.D, who conceptualized and supervised the experiments. All authors read and approved the final manuscript.

Competing interest statement

Nothing to disclose

461 **References**

462 Ackermans, M.T., Kettelarij-Haas, Y., Boelen, A., and Endert, E. (2012). Determination of thyroid
463 hormones and their metabolites in tissue using SPE UPLC-tandem MS. Biomed. Chromatogr. *26*,
464 485–490.

465 Aguirre, A., Rubio, M.E., and Gallo, V. (2010). Notch and EGFR pathway interaction regulates neural
466 stem cell number and self-renewal. Nature *467*, 323–327.

467 Amano, I., Takatsuru, Y., Khairinisa, M.A., Kokubo, M., Haijima, A., and Koibuchi, N. (2018).
468 Effects of Mild Perinatal Hypothyroidism on Cognitive Function of Adult Male Offspring.
469 Endocrinology *159*, 1910–1921.

470 Ausó, E., Lavado-Autric, R., Cuevas, E., del Rey, F.E., Morreale de Escobar, G., and Berbel, P.
471 (2004). A Moderate and Transient Deficiency of Maternal Thyroid Function at the Beginning of Fetal
472 Neocorticogenesis Alters Neuronal Migration. Endocrinology *145*, 4037–4047.

473 Azim, K., Fischer, B., Hurtado-Chong, A., Draganova, K., Cantù, C., Zemke, M., Sommer, L., Butt,
474 A., and Raineteau, O. (2014). Persistent Wnt/β-Catenin Signaling Determines Dorsalization of the
475 Postnatal Subventricular Zone and Neural Stem Cell Specification into Oligodendrocytes and
476 Glutamatergic Neurons. Stem Cells *32*, 1301–1312.

477 Bárez-López, S., and Guadaño-Ferraz, A. (2017). Thyroid Hormone Availability and Action during
478 Brain Development in Rodents. Front. Cell. Neurosci. *11*, 240.

479 Baser, A., Skabkin, M., Kleber, S., Dang, Y., Gülcüler Balta, G.S., Kalamakis, G., Göpferich, M.,
480 Ibañez, D.C., Schefzik, R., Lopez, A.S., et al. (2019). Onset of differentiation is post-transcriptionally
481 controlled in adult neural stem cells. Nature *566*, 100–104.

482 Bianco, A.C., Dumitrescu, A., Gereben, B., Ribeiro, M.O., Fonseca, T.L., Fernandes, G.W., and
483 Bocco, B.M.L.C. (2019). Paradigms of Dynamic Control of Thyroid Hormone Signaling. Endocr.
484 Rev. *40*, 1000–1047.

485 Boas, M., Feldt-Rasmussen, U., and Main, K.M. (2012). Thyroid effects of endocrine disrupting

chemicals. Mol. Cell. Endocrinol. *355*, 240–248.

Borrett, M.J., Innes, B.T., Jeong, D., Tahmasian, N., Storer, M.A., Bader, G.D., Kaplan, D.R., and Miller, F.D. (2020). Single-Cell Profiling Shows Murine Forebrain Neural Stem Cells Reacquire a Developmental State when Activated for Adult Neurogenesis. Cell Rep. *32*, 108022.

Breton-Provencher, V., Lemasson, M., Peralta, M.R., and Saghatelyan, A. (2009). Interneurons Produced in Adulthood Are Required for the Normal Functioning of the Olfactory Bulb Network and for the Execution of Selected Olfactory Behaviors. J. Neurosci. *29*, 15245–15257.

Dugas, J.C., Ibrahim, A., and Barres, B.A. (2012). The T3-induced gene KLF9 regulates oligodendrocyte differentiation and myelin regeneration. Mol. Cell. Neurosci. *50*, 45–57.

Fuentealba, L.C., Rompani, S.B., Parraguez, J.I., Obernier, K., Romero, R., Cepko, C.L., and Alvarez-Buylla, A. (2015). Embryonic Origin of Postnatal Neural Stem Cells. Cell *161*, 1644–1655.

Gilbert, M.E., Goodman, J.H., Gomez, J., Johnstone, A.F.M., and Ramos, R.L. (2017). Adult hippocampal neurogenesis is impaired by transient and moderate developmental thyroid hormone disruption. Neurotoxicology *59*, 9–21.

Gothié, J., Vancamp, P., Demeneix, B., and Remaud, S. (2020). Thyroid hormone regulation of neural stem cell fate: From development to ageing. Acta Physiol. *228*, e13316.

Gothié, J.D., Sébillot, A., Luongo, C., Legendre, M., Nguyen Van, C., Le Blay, K., Perret-Jeanneret, M., Remaud, S., and Demeneix, B.A. (2017). Adult neural stem cell fate is determined by thyroid hormone activation of mitochondrial metabolism. Mol. Metab. *6*, 1551–1561.

Gyllenberg, D., Sourander, A., Surcel, H.-M., Hinkka-Yli-Salomäki, S., McKeague, I.W., and Brown, A.S. (2016). Hypothyroxinemia During Gestation and Offspring Schizophrenia in a National Birth Cohort. Biol. Psychiatry *79*, 962–970.

Hadj-Sahraoui, N., Seugnet, I., Ghorbel, M.T., and Demeneix, B. (2000). Hypothyroidism prolongs mitotic activity in the post-natal mouse brain. Neurosci. Lett. *280*, 79–82.

Hernandez, A., Morte, B., Belinchón, M.M., Ceballos, A., and Bernal, J. (2012). Critical Role of

Types 2 and 3 Deiodinases in the Negative Regulation of Gene Expression by T3 in the Mouse Cerebral Cortex. Endocrinology *153*, 2919–2928.

Ihrie, R.A., Shah, J.K., Harwell, C.C., Levine, J.H., Guinto, C.D., Lezameta, M., Kriegstein, A.R., and Alvarez-Buylla, A. (2011). Persistent Sonic Hedgehog Signaling in Adult Brain Determines Neural Stem Cell Positional Identity. Neuron *71*, 250–262.

Jacobs, M.N., Marczylo, E.L., Guerrero-Bosagna, C., and Rüegg, J. (2017). Marked for Life: Epigenetic Effects of Endocrine Disrupting Chemicals. Annu. Rev. Environ. Resour. *42*, 105–160.

Korevaar, T.I.M.M., Muetzel, R., Medici, M., Chaker, L., Jaddoe, V.W.V. V, de Rijke, Y.B., Steegers, E.A.P.P., Visser, T.J., White, T., Tiemeier, H., et al. (2016). Association of maternal thyroid function during early pregnancy with offspring IQ and brain morphology in childhood: a population-based prospective cohort study. Lancet Diabetes Endocrinol. *4*, 35–43.

Lemkine, G.F., Raji, A., Alfama, G., Turque, N., Hassani, Z., Alegria-Prévot, O., Samarut, J., Levi, G., and Demeneix, B.A. (2005). Adult neural stem cell cycling in vivo requires thyroid hormone and its alpha receptor. FASEB J. *19*, 1–17.

Lim, D.A., and Alvarez-Buylla, A. (2016). The Adult Ventricular–Subventricular Zone (V-SVZ) and Olfactory Bulb (OB) Neurogenesis. Cold Spring Harb. Perspect. Biol. *8*, a018820.

López-Espíndola, D., García-Aldea, Á., Gómez de la Riva, I., Rodríguez-García, A.M., Salvatore, D., Visser, T.J., Bernal, J., and Guadaño-Ferraz, A. (2019). Thyroid hormone availability in the human fetal brain: novel entry pathways and role of radial glia. Brain Struct. Funct. *224*, 2103–2119.

López-Juárez, A., Remaud, S., Hassani, Z., Jolivet, P., Pierre Simons, J., Sontag, T., Yoshikawa, K., Price, J., Morvan-Dubois, G., and Demeneix, B.A. (2012). Thyroid Hormone Signaling Acts as a Neurogenic Switch by Repressing Sox2 in the Adult Neural Stem Cell Niche. Cell Stem Cell *10*, 531–543.

Luongo, C., Butruille, L., Sébillot, A., Le Blay, K., Schwaninger, M., Heuer, H., Demeneix, B.A., and Remaud, S. (2021). Absence of Both Thyroid Hormone Transporters MCT8 and OATP1C1 Impairs

Neural Stem Cell Fate in the Adult Mouse Subventricular Zone. Stem Cell Reports *16*, 337–353.

Mayerl, S., Heuer, H., and Ffrench-Constant, C. (2020). Hippocampal Neurogenesis Requires Cell-Autonomous Thyroid Hormone Signaling. Stem Cell Reports *14*, 845–860.

McKenzie, I.A., Ohayon, D., Li, H., Paes de Faria, J., Emery, B., Tohyama, K., and Richardson, W.D. (2014). Motor skill learning requires active central myelination. Science (80-.). *346*, 318–322.

Menn, B., Garcia-Verdugo, J.M., Yaschine, C., Gonzalez-Perez, O., Rowitch, D., and Alvarez-Buylla, A. (2006). Origin of Oligodendrocytes in the Subventricular Zone of the Adult Brain. J. Neurosci. *26*, 7907–7918.

Merkle, F.T., Tramontin, A.D., Garcia-Verdugo, J.M., and Alvarez-Buylla, A. (2004). Radial glia give rise to adult neural stem cells in the subventricular zone. Proc. Natl. Acad. Sci. *101*, 17528–17532.

Mizrak, D., Levitin, H.M., Delgado, A.C., Crotet, V., Yuan, J., Chaker, Z., Silva-Vargas, V., Sims, P.A., and Doetsch, F. (2019). Single-Cell Analysis of Regional Differences in Adult V-SVZ Neural Stem Cell Lineages. Cell Rep. *26*, 394-406.e5.

Monk, J.A., Sims, N.A., Dziegielewska, K.M., Weiss, R.E., Ramsay, R.G., and Richardson, S.J. (2013). Delayed development of specific thyroid hormone-regulated events in transthyretin null mice. Am. J. Physiol. Metab. *304*, E23–E31.

Montero-Pedrazuela, A., Venero, C., Lavado-Autric, R., Fernández-Lamo, I., García-Verdugo, J.M., Bernal, J., and Guadaño-Ferraz, A. (2006). Modulation of adult hippocampal neurogenesis by thyroid hormones: implications in depressive-like behavior. Mol. Psychiatry *11*, 361–371.

Moog, N.K., Entringer, S., Heim, C., Wadhwa, P.D., Kathmann, N., and Buss, C. (2017). Influence of maternal thyroid hormones during gestation on fetal brain development. Neuroscience *342*, 68–100.

Mughal, B.B., Fini, J.-B., and Demeneix, B.A. (2018). Thyroid-disrupting chemicals and brain development: an update. Endocr. Connect. *7*, R160–R186.

O'Shaughnessy, K.L., Kosian, P.A., Ford, J.L., Oshiro, W.M., Degitz, S.J., and Gilbert, M.E. (2018). Developmental Thyroid Hormone Insufficiency Induces a Cortical Brain Malformation and Learning

561 Impairments: A Cross-Fostering Study. Toxicol. Sci. *163*, 101–115.

562 Ramhøj, L., Hass, U., Gilbert, M.E., Wood, C., Svingen, T., Usai, D., Vinggaard, A.M., Mandrup, K.,
563 and Axelstad, M. (2020). Evaluating thyroid hormone disruption: investigations of long-term
564 neurodevelopmental effects in rats after perinatal exposure to perfluorohexane sulfonate (PFHxS). Sci.
565 Rep. *10*, 2672.

566 Remaud, S., Ortiz, F.C., Perret-Jeanneret, M., Aigrot, M.-S., Gothié, J.-D., Fekete, C., Kvárta-Papp,
567 Z., Gereben, B., Langui, D., Lubetzki, C., et al. (2017). Transient hypothyroidism favors
568 oligodendrocyte generation providing functional remyelination in the adult mouse brain. Elife *6*,
569 e29996.

570 Roberts, L.M., Woodford, K., Zhou, M., Black, D.S., Haggerty, J.E., Tate, E.H., Grindstaff, K.K.,
571 Mengesha, W., Raman, C., and Zerangue, N. (2008). Expression of the Thyroid Hormone Transporters
572 Monocarboxylate Transporter-8 (SLC16A2) and Organic Ion Transporter-14 (SLCO1C1) at the
573 Blood-Brain Barrier. Endocrinology *149*, 6251–6261.

574 Rushing, G., and Ihrie, R.A. (2016). Neural stem cell heterogeneity through time and space in the
575 ventricular-subventricular zone. Front. Biol. (Beijing). *11*, 261–284.

576 Skah, S., Uchuya-Castillo, J., Sirakov, M., and Plateroti, M. (2017). The thyroid hormone nuclear
577 receptors and the Wnt/β-catenin pathway: An intriguing liaison. Dev. Biol. *422*, 71–82.

578 Stuart, T., Butler, A., Hoffman, P., Hafemeister, C., Papalexi, E., Mauck, W.M., Hao, Y., Stoeckius,
579 M., Smibert, P., and Satija, R. (2019). Comprehensive Integration of Single-Cell Data. Cell *177*, 1888-
580 1902.e21.

581 Tong, H., Chen, G.-H., Liu, R.-Y., and Zhou, J.-N. (2007). Age-related learning and memory
582 impairments in adult-onset hypothyroidism in Kunming mice. Physiol. Behav. *91*, 290–298.

583 Vancamp, P., Gothié, J.-D., Luongo, C., Sébillot, A., Le Blay, K., Butruille, L., Pagnin, M.,
584 Richardson, S.J., Demeneix, B.A., and Remaud, S. (2019). Gender-specific effects of transthyretin on
585 neural stem cell fate in the subventricular zone of the adult mouse. Sci. Rep. *9*, 19689.

586 Vancamp, P., Butruille, L., Demeneix, B.A., and Remaud, S. (2020a). Thyroid Hormone and Neural
587 Stem Cells: Repair Potential Following Brain and Spinal Cord Injury. Front. Neurosci. *14*, 875.

588 Vancamp, P., Demeneix, B.A., and Remaud, S. (2020b). Monocarboxylate Transporter 8 Deficiency:
589 Delayed or Permanent Hypomyelination? Front. Endocrinol. (Lausanne). *11*, 283.

590 de Vries, E.M., Surovtseva, O., Vos, W.G., Kunst, R.F., van Beeren, M., Kwakkel, J., Chassande, O.,
591 Ackermans, M.T., Fliers, E., and Boelen, A. (2019). Downregulation of Type 3 Deiodinase in the
592 Hypothalamus During Inflammation. Thyroid *29*, 1336–1343.

593 Williams, G.R. (2008). Neurodevelopmental and Neurophysiological Actions of Thyroid Hormone. J.
594 Neuroendocrinol. *20*, 784–794.

595 Wilpert, N.-M., Krueger, M., Opitz, R., Sebinger, D., Paisdzior, S., Mages, B., Schulz, A., Spranger,
596 J., Wirth, E.K., Stachelscheid, H., et al. (2020). Spatiotemporal Changes of Cerebral Monocarboxylate
597 Transporter 8 Expression. Thyroid *30*, 1366–1383.

598 Xu, M., Huang, Y., Li, K., Cheng, X., Li, G., Liu, M., Nie, Y., Geng, S., and Zhao, S. (2018).
599 Developmental exposure of decabromodiphenyl ether impairs subventricular zone neurogenesis and
600 morphology of granule cells in mouse olfactory bulb. Arch. Toxicol. *92*, 529–539.

601 Zhang, L., Blomgren, K., Kuhn, H.G., and Cooper-Kuhn, C.M. (2009). Effects of postnatal thyroid
602 hormone deficiency on neurogenesis in the juvenile and adult rat. Neurobiol. Dis. *34*, 366–374.

603 Zhang, S., Zhu, X., Gui, X., Croteau, C., Song, L., Xu, J., Wang, A., Bannerman, P., and Guo, F.
604 (2018). Sox2 Is Essential for Oligodendroglial Proliferation and Differentiation during Postnatal Brain
605 Myelination and CNS Remyelination. J. Neurosci. *38*, 1802–1820.

606 Zywitza, V., Misios, A., Bunatyan, L., Willnow, T.E., and Rajewsky, N. (2018). Single-Cell
607 Transcriptomics Characterizes Cell Types in the Subventricular Zone and Uncovers Molecular Defects
608 Impairing Adult Neurogenesis. Cell Rep. *25*, 2457-2469.e8.

609

Figures titles and legends

Figure 1. Cellular reorganization and dynamic expression of TH pathway and neuroglial genes in SVZ cell populations at P2 and P20. (**A**) Two-dimensional UMAP plots showing five isolated SVZ-cell clusters of interest at P2 and P20 after integrated single-cell RNA-Seq re-analysis (See also Fig. S1). The lower panel shows the proportion of each cell type relative to total cell numbers. (**B**) Violin plots showing expression of the TH transporters *Mct8* and *Oatp1c1*, the deiodinases *Dio2* and *Dio3* and the two TR encoding genes *Thra* and *Thrb* in the SVZ-cell clusters at P2 (red) and P20 (dark green) (See also Fig. S2). (**C**) Clusters plots mapping cell-specific expression patterns of *Mct8* and *Oatp1c1*, and *Dio2* and *Dio3* (See also Fig. S3, S4). (**D**) Violin plots showing expression of the positively and negatively TH-regulated genes *Klf9* and *Msi1*, respectively, the pro-oligodendrogenic genes *Olig2* and *Ng2* and the pro-neuronal genes *Dlx2* and *Dcx*. (**E**) Schematic overview of the P4 and P21 SVZ (area within white dotted lines). (**F**) Representative RNAscope pictures showing expression of TH-regulated genes in SOX2+ SVZ-progenitors (white circles). Scale bars: 50 µm, inserts 10 µm. (**G**) Pictures showing TRα1 in SOX2+ SVZ-progenitors. White arrows mark co-expression. Scale bar = 10 µm. CC: corpus callosum; NB: neuroblasts; NSC: neural stem cells; OPC: oligodendrocyte precursor cell; St: striatum; SVZ: subventricular zone; TAP: transient amplifying progenitor; v: ventricle. (See also Figure S1, S2, S3 and S4).

Figure 2. Developmental PTU treatment alters expression of TH regulator genes and markers for neuroglia commitment. (**A**) Graph showing slower weight gain in hypothyroid newborn mice at P15-P21. (**B**) Graphs showing serum T_4 and T_3 levels (nmol/L) at P4 and P15 in CTL- and PTU-treated mice (n = 3-6). (**C**) Heat-map showing relative changes (Log-transformed data) in expression of genes (blue) within the TH signaling pathway and those implicated in NSC commitment, as compared to control animals at P4 for each gene (set to 0). n = 4-6/group (N = 3/replicate), two-way ANOVAs followed by Šidák post-hoc tests (see Fig. S2 for fold changes). (**D**) Representative RNAscope pictures showing TH-target gene expression in SOX2+ SVZ-progenitors (white circles) in CTL and PTU animals at P21. Each yellow dot represents one mRNA transcript (white arrows) (n = 3-

4/group, *Dio2* & *Klf9*: two-tailed t-tests; *Dio3*: Mann-Whitney U test). Scale bars: 10 µm. (see also Table S1).

Figure 3. Developmental PTU treatment affects SVZ neurogliogenesis at P21. (**A**) Representative IHC pictures for DCX+ neuroblasts (red) and OLIG2+ OPCs (green) on coronal sections of the dorsal SVZ. At P4, almost exclusively OLIG2+ OPCs are observed (left panels). Counts were performed in the area delineated by the red boxes, on 3-4 sections/animal. A burst of DCX+ neuroblasts was observed at P21 (right panels). Scale bars: 50 µm. (**B**) Graphs showing densities of OLIG2+ and DCX+ cells in the dorsal SVZ (area within white dotted lines in **A**). (**C**) Representative IHC pictures for DCX+ neuroblasts and OLIG2+ OPCs on coronal sections of the LV-SVZ. Scale bars: 20 µm. (**D**) Graphs showing the numbers of OLIG2+ cells and DCX+ cells (per mm) in the LV-SVZ. (**E**) The neuro/glia balance was calculated as the ratio between DCX+/DCX+OLIG2+ cells *vs.* OLIG2+/DCX+OLIG2+ cells. Plots depicting mean ± SD. n = 5-8/group, two-way ANOVAs followed by Tukey post-hoc tests. CC: corpus callosum; dSVZ: dorsal subventricular zone; LV-SVZ: lateroventral subventricular zone; st: striatum; v: ventricle.

Figure 4. Developmental PTU treatment increases SOX2+ progenitors and reduces mitosis in the postnatal SVZ. (**A**) Representative IHC pictures for PH3+ mitotic cells (green) and SOX2+ progenitors (red) on coronal sections of the dorsal SVZ. Scale bars: 50 µm. (**B**) Graphs showing densities of PH3+ and SOX2+ cells in the dorsal SVZ (area within white dotted lines in **A**). (**C**) Representative IHC pictures for PH3+ mitotic cells and SOX2+ progenitors on coronal sections of the LV-SVZ. Scale bars: 20 µm. (**D**) Graphs showing numbers of PH3+ and SOX2+ cells (per mm) in the LV-SVZ. Plots depicting mean ± SD. n = 4-8/group, two-way ANOVAs followed by Tukey post-hoc tests. CC: corpus callosum; dSVZ: dorsal subventricular zone; LV-SVZ: lateroventral subventricular zone; st: striatum; v: ventricle.

Figure 5. T_3 affects neither the neuro/glia balance nor differentiation in SVZ-NSC/progenitors from PTU-treated mice. (**A**) Schematic representation of the neurosphere assay. (**B**) Representative IHC pictures of DCX+ neuroblasts (red) and OLIG2+ OPCs (green), differentiated from SVZ-NSC/progenitors isolated from CTL- and PTU-treated P4 animals. Scale bar: 10 µm. (**C**) Graphs showing the proportion of DCX+ or OLIG2+ cells in the DAPI+ cell population at P4. (**D**) Representative pictures of DCX+ neuroblasts and OLIG2+ OPCs, differentiated from SVZ-NSC/progenitors isolated from CTL- and PTU-treated P21 animals. Notice the lower proportion of differentiated cells in the lower left panel (CTL, 50 nM T_3), and reduced DCX+ neuroblasts. (**E**) Graphs showing the proportion of DCX+ or OLIG2+ cells in the DAPI+ cell population at P21. (**F)** Graphs showing the ratio of DCX+ *vs.* OLIG2+ cells, reflecting the neuro/glia balance. Plots depicting mean ± SD. N = 24-30 images/group, data from n = 3 independent experiments. Two-way ANOVAs followed by Tukey post-hoc tests. DIV: days *in vitro*; SVZ-NSC: subventricular zone-derived neural stem cell.

Figure 6. Impaired short-term olfactory memory and olfactory bulb cyto-architecture in adult mice developmentally exposed to PTU. (**A**) Graphs showing weight and serum T_4, T_3 and rT_3 levels (nmol/L) in P100 control mice and those developmentally treated with PTU (n = 5/group). (**B**) Left graph (habituation-dishabituation test) showing investigation time following three consecutive presentations of odors relative to water. The right graph (short-term odor memory test) shows the relative investigation time 2 (habituation), 30 and 60 min after presentation of the same odor (short-term memory). Graphs depict mean ± SEM (n = 5/group, Bonferroni post-hoc test following two-way ANOVAs). Asterisks mark differences between groups at one time point, letters between time points within one group. (**D**) Representative IHC pictures in the glomerular layer (white dotted lines) of the olfactory bulb (red box on schematic section) for tyrosine hydroxylase+ (red, left pictures), calretinin+ (green, right pictures) and calbindin+ neurons (red, right pictures). Scale bars: 50 µm. (**E**) Graphs showing neuronal densities in the glomerular layer (n = 5/group, unpaired t tests). The right, lower graph shows the relative proportions of neuronal subtypes. Plots depicting mean ± SD. CALB:

calbindin; CALR: calretinin; EPL: external plexiform layer; GL: glomerular layer; ONL: olfactory nerve layer; TYR: tyrosine hydroxylase.

Figure 7. Reduced SVZ-oligodendrogenesis in adult mice developmentally exposed to PTU. (**A**) Representative images of the dorsal (left panels, scale bars: 20 µm) and LV-SVZ (right panels, scale bars: 10 µm) showing DCX+ neuroblasts (red) and OLIG2+ oligodendroglia (green). (**B**) Graphs showing DCX+ and OLIG2+ cell densities in the dorsal (left) and numbers per mm in the LV-SVZ (right) (n = 5/group, unpaired t tests). (**C**) Relative proportions of DCX+ *vs.* OLIG2+ cells reflecting the neuro/glia balance. (**D**) Representative images of the dorsal (left panels, scale bars: 20 µm) and lateral SVZ (right panels, scale bars: 10 µm) showing SOX2+ (light blue), PH3+ (green) and Ki67+ cells (red). (**E**) Graphs showing SOX2+ and Ki67+ cell densities in the dorsal (left) and numbers per mm in the LV-SVZ (right) (n = 5, unpaired t tests, Mann-Whitney U test for the upper left graph) (**F**) Pie diagrams showing the proliferation index (PH3+Ki67+/Ki67+ cells). CC: corpus callosum; dSVZ: dorsal subventricular zone; LV-SVZ: lateroventral subventricular zone; PI: proliferation index. St: striatum; v: ventricle.

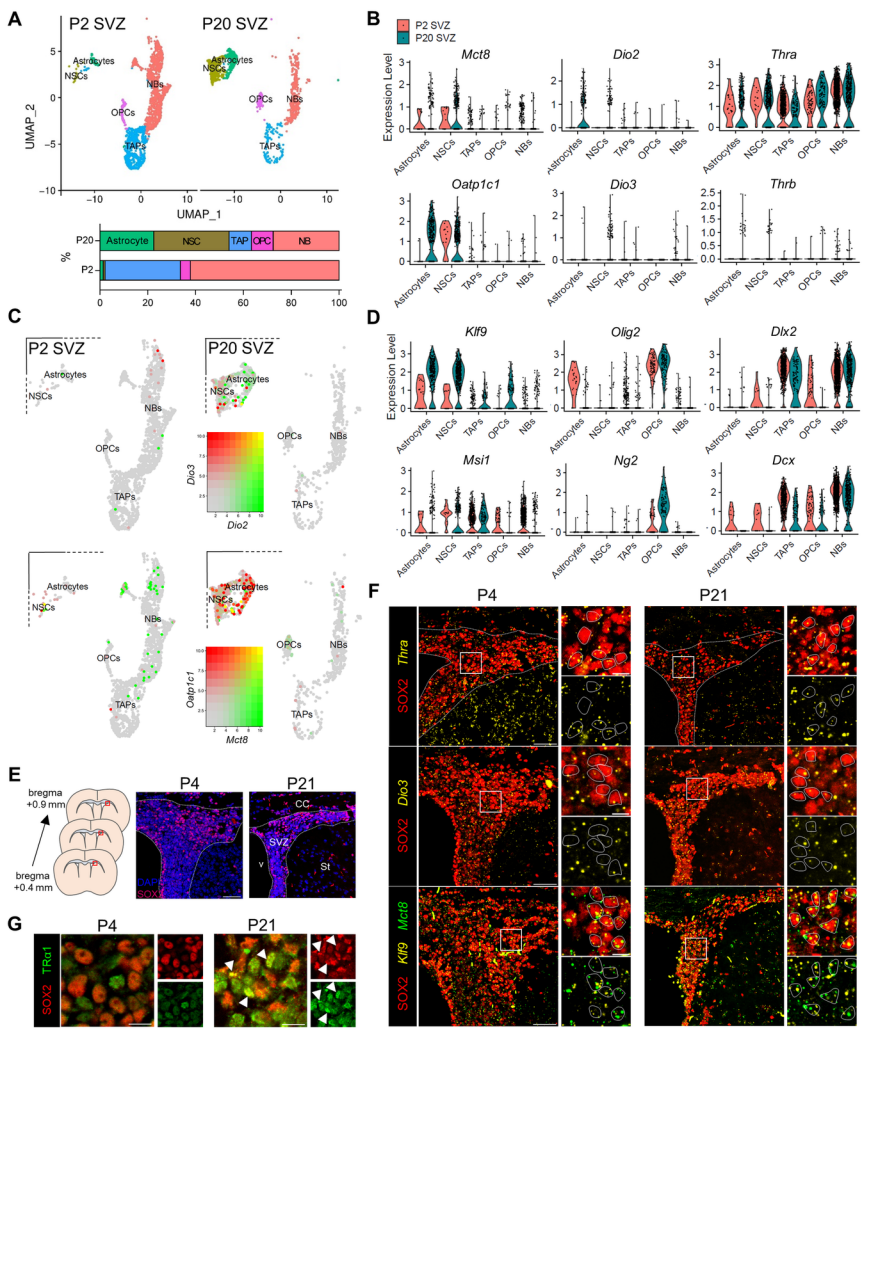
A
P2 SVZ
P20 SVZ
Astrocytes
NSCs
NBs
OPCs
TAPs
UMAP_2
UMAP_1
P20
P2
%
Astrocyte
NSC
TAP
OPC
NB
B
P2 SVZ
P20 SVZ
Expression Level
Mct8
Dio2
Thra
Oatp1c1
Dio3
Thrb
Astrocytes
NSCs
TAPs
OPCs
NBs
C
Dio3
Dio2
Oatp1c1
Mct8
D
Klf9
Olig2
Dlx2
Msi1
Ng2
Dcx
E
bregma +0.9 mm
bregma +0.4 mm
P4
P21
DAPI
SOX2
CC
SVZ
V
St
F
SOX2
Thra
Dio3
Mct8
Klf9
G
TRα1

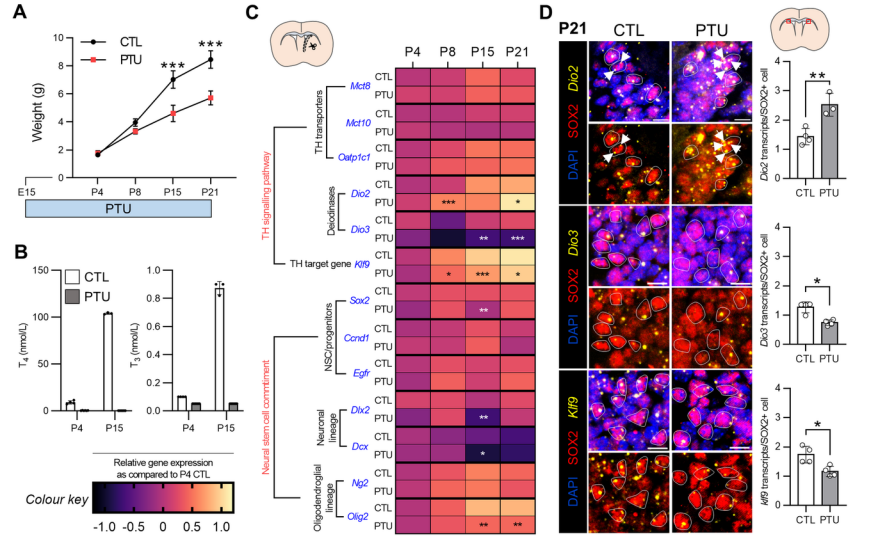
A
CTL
PTU
Weight (g)
***
***
E15
P4
P8
P15
P21
PTU
B
CTL
PTU
T4 (nmol/L)
T3 (nmol/L)
P4
P15
Relative gene expression as compared to P4 CTL
Colour key
-1.0 -0.5 0 0.5 1.0
C
P4
P8
P15
P21
TH signalling pathway
Neural stem cell commitment
TH transporters
Mct8
Mct10
Oatp1c1
Deiodinases
Dio2
Dio3
TH target gene Klf9
NSC/progenitors
Sox2
Ccnd1
Egfr
Neuronal lineage
Dlx2
Dcx
Oligodendroglial lineage
Ng2
Olig2
CTL
PTU
D
P21
CTL
PTU
Dio2
SOX2
DAPI
Dio3
Klf9
Dio2 transcripts/SOX2+ cell
Dio3 transcripts/SOX2+ cell
Klf9 transcripts/SOX2+ cell

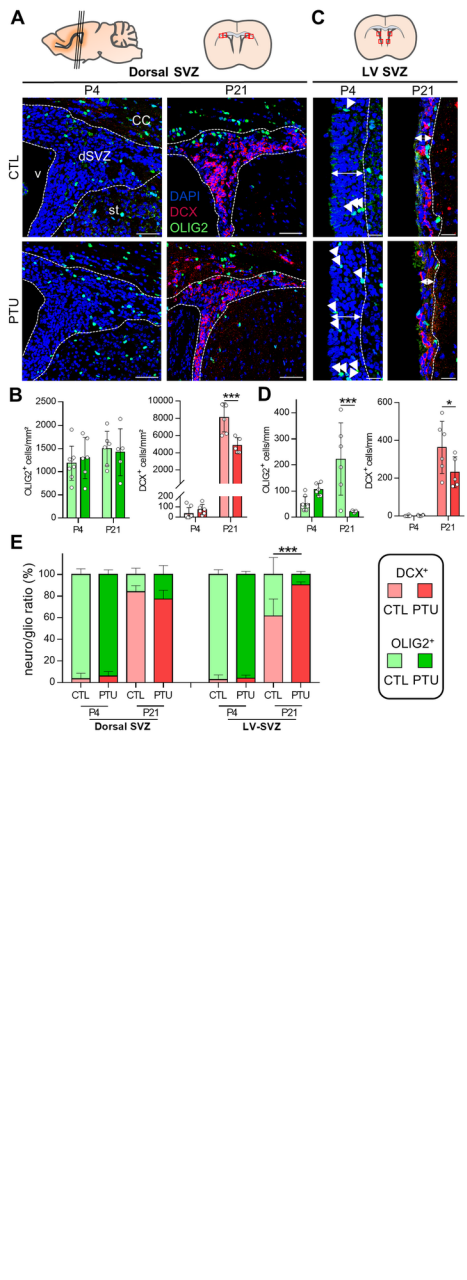
A
Dorsal SVZ
C
LV SVZ
P4
P21
P4
P21
CC
dSVZ
v
st
CTL
PTU
DAPI
DCX
OLIG2
B
OLIG2+ cells/mm²
DCX+ cells/mm²
***
P4
P21
D
OLIG2+ cells/mm
DCX+ cells/mm
***
*
P4
P21
E
neuro/glio ratio (%)
***
CTL
PTU
P4
P21
Dorsal SVZ
LV-SVZ
DCX+
CTL PTU
OLIG2+
CTL PTU

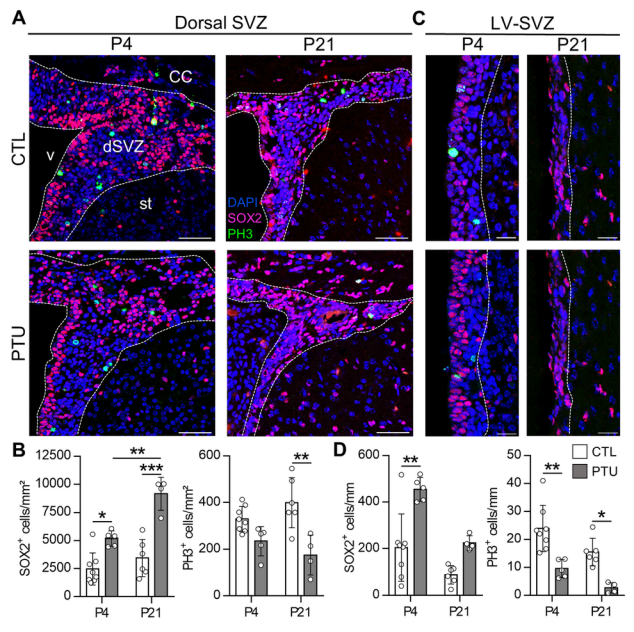
A
Dorsal SVZ
P4
P21
C
LV-SVZ
P4
P21
CTL
PTU
CC
dSVZ
v
st
DAPI
SOX2
PH3
B
SOX2+ cells/mm²
PH3+ cells/mm²
D
SOX2+ cells/mm
PH3+ cells/mm
CTL
PTU
P4
P21

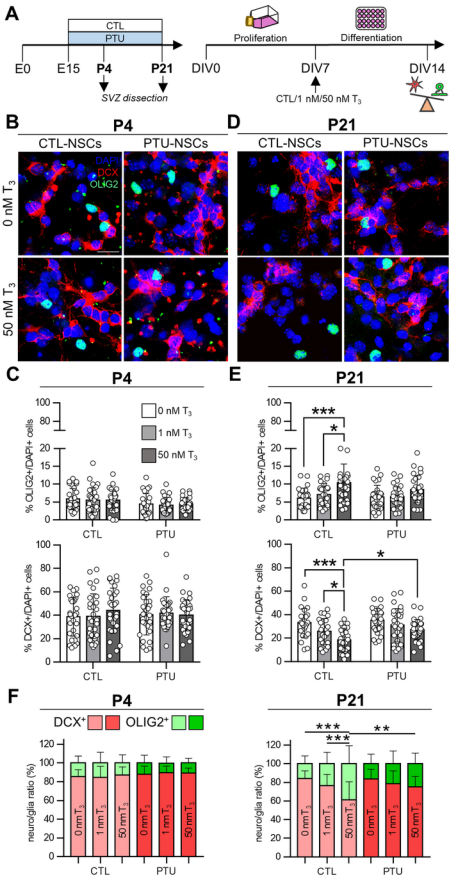
A
CTL
PTU
E0
E15
P4
P21
SVZ dissection
DIV0
Proliferation
Differentiation
DIV7
DIV14
CTL/1 nM/50 nM T3
B
P4
CTL-NSCs
PTU-NSCs
DAPI
DCX
OLIG2
0 nM T3
50 nM T3
D
P21
CTL-NSCs
PTU-NSCs
C
P4
0 nM T3
1 nM T3
50 nM T3
% OLIG2+/DAPI+ cells
% DCX+/DAPI+ cells
CTL
PTU
E
P21
***
*
F
P4
DCX+
OLIG2+
neuro/glia ratio (%)
0 nM T3
1 nM T3
50 nM T3
P21
**

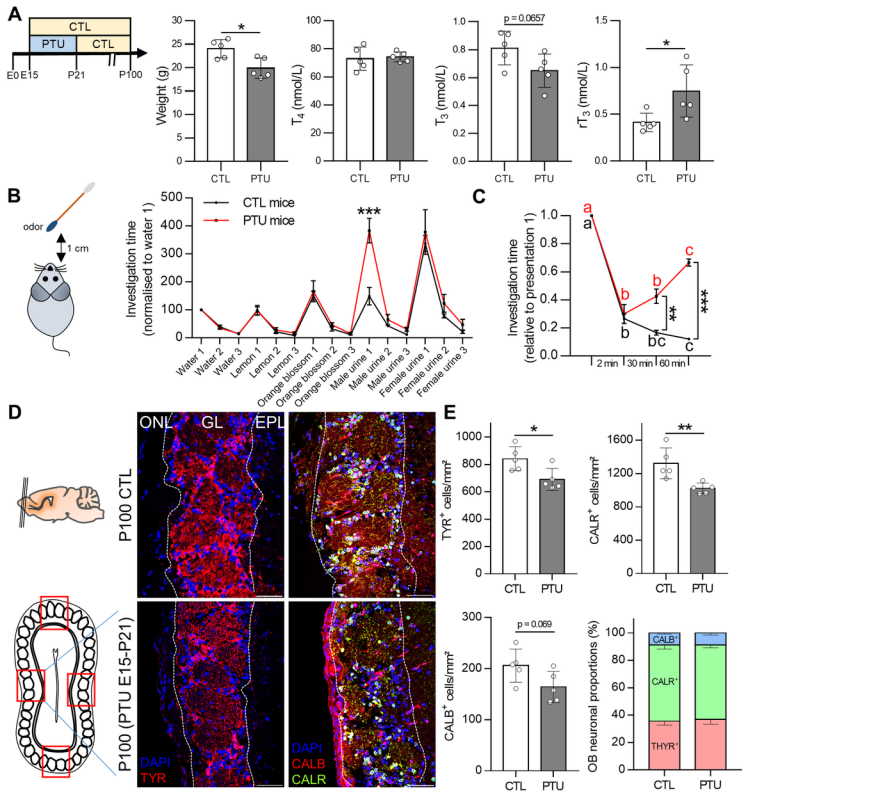
A
CTL
PTU
CTL
E0 E15
P21
P100
Weight (g)
T4 (nmol/L)
T3 (nmol/L)
p = 0.0657
rT3 (nmol/L)
CTL
PTU
B
odor
1 cm
CTL mice
PTU mice
***
Investigation time (normalised to water 1)
Water 1
Water 2
Water 3
Lemon 1
Lemon 2
Lemon 3
Orange blossom 1
Orange blossom 2
Orange blossom 3
Male urine 1
Male urine 2
Male urine 3
Female urine 1
Female urine 2
Female urine 3
C
Investigation time (relative to presentation 1)
a
b
c
**
***
2 min
30 min
60 min
D
ONL
GL
EPL
P100 CTL
P100 (PTU E15-P21)
DAPI
TYR
DAPI
CALB
CALR
E
TYR+ cells/mm²
CALR+ cells/mm²
p = 0.069
CALB+ cells/mm²
OB neuronal proportions (%)
CALB+
CALR+
THYR+
CTL
PTU

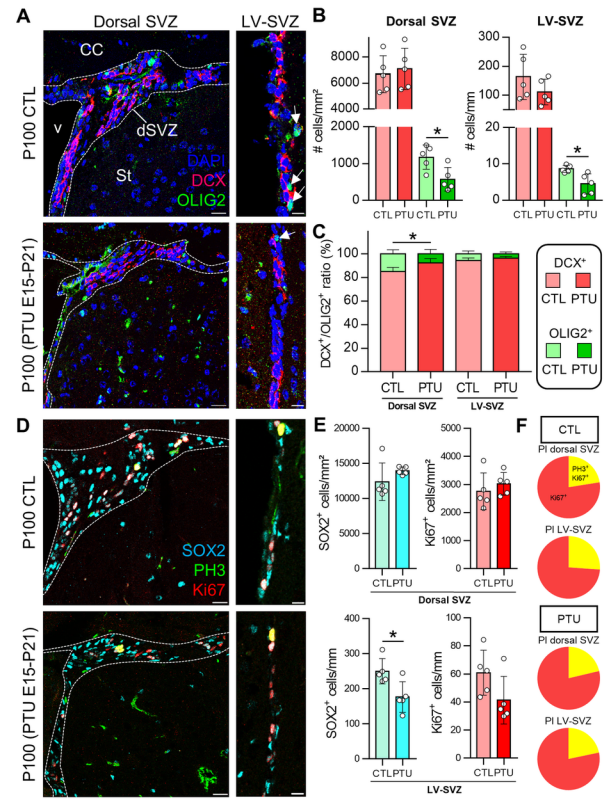
A
Dorsal SVZ
LV-SVZ
P100 CTL
P100 (PTU E15-P21)
CC
v
dSVZ
St
DAPI
DCX
OLIG2
B
Dorsal SVZ
LV-SVZ
cells/mm²
cells/mm
CTL PTU CTL PTU
C
DCX⁺/OLIG2⁺ ratio (%)
CTL PTU CTL PTU
Dorsal SVZ
LV-SVZ
DCX⁺
OLIG2⁺
D
SOX2
PH3
Ki67
E
SOX2⁺ cells/mm²
Ki67⁺ cells/mm²
SOX2⁺ cells/mm
Ki67⁺ cells/mm
CTL PTU
Dorsal SVZ
LV-SVZ
F
CTL
PTU
PI dorsal SVZ
PI LV-SVZ
PH3⁺ Ki67⁺
Ki67⁺

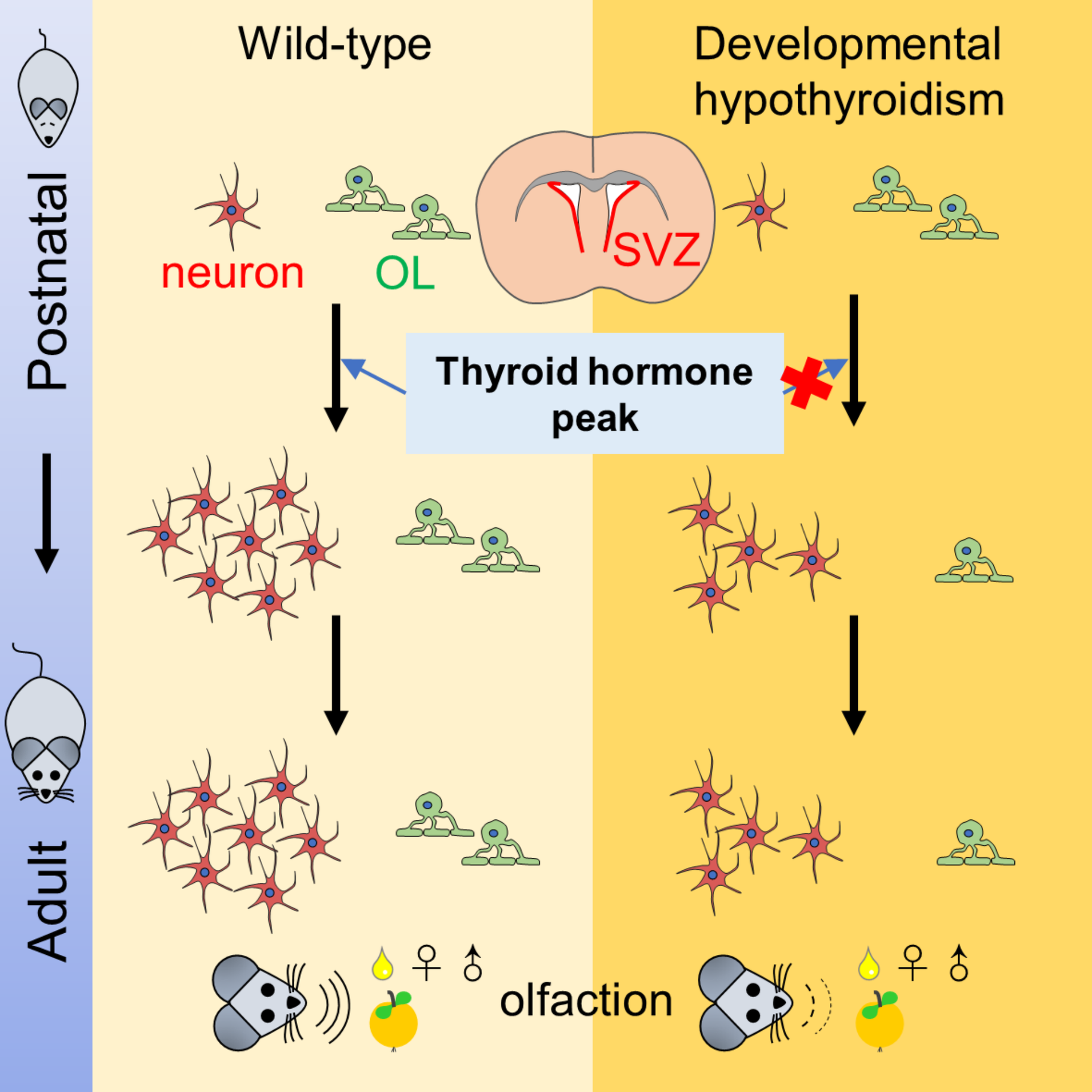
Wild-type
Developmental hypothyroidism
Postnatal
Adult
neuron
OL
SVZ
Thyroid hormone peak
olfaction